Full Length Article

Nature of the Pt-Cobalt-Oxide surface interaction and its role in the CO$_2$ Methanation

Anastasiia Efremova [a],[1], Imre Szenti [a],[1], János Kiss [a],[b], Ákos Szamosvölgyi [a], András Sápi [a],[*], Kornélia Baán [a], Luca Olivi [c], Gábor Varga [d], Zsolt Fogarassy [e], Béla Pécz [e], Ákos Kukovecz [a], Zoltán Kónya [a],[b]

[a] *University of Szeged, Interdisciplinary Excellence Centre, Department of Applied and Environmental Chemistry, H-6720, Rerrich Béla tér 1, Szeged, Hungary*
[b] *MTA-SZTE Reaction Kinetics and Surface Chemistry Research Group, Rerrich Béla tér 1, Szeged H-6720, Hungary*
[c] *Elettra Sicrotrone Trieste, Strada Statale 14 - km, in AREA Science Park, 34149 Basovizza, Italy*
[d] *Department of Physical Chemistry and Materials Science, University of Szeged, Rerrich Béla tér 1, Szeged 6720, Hungary*
[e] *Centre for Energy Research, Institute for Technical Physics and Materials Science, Konkoly-Thege M. út 29-33., Budapest 1121, Hungary*

ARTICLE INFO

ABSTRACT

Based on our previous investigations, it turned out that the Co$_3$O$_4$ material is a promising catalyst in the ambient pressure CO$_2$ methanation. This work aims at understanding the Pt-Cobalt-Oxide surface interaction and its effect on the catalytic performance. The incorporation of Pt nanoparticles into the mesoporous Co$_3$O$_4$ (Pt/m-Co$_3$O$_4$) and commercial Co$_3$O$_4$ (Pt/c-Co$_3$O$_4$) improves the catalytic activity of both catalysts by a factor of ∼ 1.4 and ∼ 1.9 respectively at 673 K. The same tendency towards the increased basicity was also observed. Morphology-induced surface basicity was previously shown to play a key role in determining the catalytic activity of free-standing supports. From HR-TEM (-EDX), EXAFS, CO$_2$-TPD, and CO chemisorption measurements it was established that during the pre-treatment, Co-Pt alloy particles partially covered by the Co$_x$O$_y$ layer are formed. It has been postulated that this structure transformation generates new basic centres, the amount of which per unit surface area is significantly larger for Pt/c-Co$_3$O$_4$ and this in turn is responsible for the higher enhancement effect of the Pt/c-Co$_3$O$_4$ catalyst in the CO$_2$ methanation. This study emphasizes the importance of the surface structure exploration for the dynamic catalytic systems in order to reach maximum activity and selectivity in the CO$_2$ methanation.

1. Introduction

The rapid development of technical and technological applications over the past few centuries has been accompanied by the utilization of carbon fuels, injudicious deforestation, and the decrease of green spaces. This has brought about an increase in the amount of carbon dioxide in the Earth´s biosphere, which is associated with the adverse effects on climate change [1,2].

The major hurdle for CO$_2$ utilization is the thermodynamic stability of the carbon dioxide molecule and the high endothermicity of its involvement in chemical interactions [3–5]. Heterogeneous catalytic hydrogenation not only opens a perspective way to involve cheap, safe, and renewable CO$_2$ source into a chemical interaction but also allows the production of valuable synthetic fuel components, such as methane.

Co-containing catalysts with the active Cobalt phase are particularly active in the conversion of carbon dioxide to methane [6–8], however, modification of Cobalt species can shift the selectivity towards carbon monoxide [9,10], methanol [11] or even light olefins [12]. The detailed research in the field proposed such factors as morphology [9], surface orientation [13], catalyst support [10], chemical state of Co species [8,14] ensemble effect [15] to be decisive in determining the activity and selectivity of CO$_2$ methanation over Co-based catalysts. The Cobalt oxide containing catalysts, including their Pt metal-modified structures are in the focus of heterogeneous catalytic and electrocatalytic applications, therefore their morphology and surface chemistry characterization are the subject of recent investigations [16–18].

In our previous work [14], we have studied bulk and surface properties of mesoporous and commercial Co$_3$O$_4$ material (m-Co$_3$O$_4$ and c-

---

Co_3O_4 correspondingly) to derive the catalytic performance correlations, which is further impeded by the structural complexity and dynamism of the Co_3O_4 system under reductive CO_2 hydrogenation environment. Though both supports showed high CH_4-selectivity, notable differences in reducibility, basic character, and tendency to form oxygen vacancies were observed, which resulted in distinct mechanisms. Emergence of additional formate route contributing to the overall methane production on m-Co_3O_4 was attributed to the presence of morphology-induced weak basic sites, aiding for the CO_2 adsorption.

The deposition of size-controlled Pt nanoparticles improved the catalytic activity of both catalysts with the slight decrease in methane selectivity [14]. This may be simply assigned to the effects of H_2-spillover and/or to the increased number of active centres at the Pt/support interphase responsible for CO formation [19,20]. However, the increase in the catalytic performance was considerably higher than increase in the CO selectivity, which means that Pt nanoparticles contribute to the CH_4 formation as well. Moreover, the enhancement effect of Pt nanoparticles was not equal and more pronounced in the case of c-Co_3O_4. This suggests more complex interactions of Pt nanoparticles with the Co_3O_4 support than mere creating a new interphase.

Thus, this study focuses on utilizing m-Co_3O_4 and c-Co_3O_4 supported 1 % 5 nm Pt nanoparticles catalysts to probe the enhancement effect of Pt nanoparticles in the CO_2 methanation. The resulting catalysts were denoted as Pt/m-Co_3O_4 and Pt/c-Co_3O_4. A detailed understanding of the catalysts' structure was obtained by a combination of surface sensitive and bulk techniques such as X-Ray Photoelectron Spectroscopy (XPS), In-Situ Diffuse Reflectance Infrared Fourier Transform Spectroscopy (DRIFTS), X-Ray Absorption Fine Structure Spectroscopy (XAFS), High Resolution Transmission Electron Microscopy (HR-TEM), High-angle annular dark-field scanning transmission electron microscopy (HAADF-STEM). We found that during the pre-treatment process a formation of the complex structure occurs, in which Co-Pt alloy particles are partially covered by Co_xO_y islets. We suggest that this structural rearrangement creates new basic centres, which are responsible for the higher enhancement effect of the Pt/c-Co_3O_4 in the CO_2 methanation.

2. Material and methods

2.1. Preparation of the catalysts

Details for all the experimental procedures are given in our previous work [14]. Shortly, the synthesis of 5 nm Pt nanoparticles was conducted through polyol method by combining 50 mg of $H_2PtCl_6 \cdot 6H_2O$ and 220 mg of PVP, each dissolved in 10 ml of ethylene–glycol. After thorough mixing, the particles were precipitated with 40 ml of acetone, washed, and redispersed in 10 ml of ethanol.

Mesoporous cobalt oxide (m-Co_3O_4) was prepared through hard template method by mixing 4.65 g $Co(NO_3)_2 \cdot 6H_2O$ in 8 ml of water with a suspension of 4 g KIT-6 silica in 50 ml of toluene [21]. After the evaporation of toluene, the precipitated product was dried and calcined at 573 K for 6 h. The silica template was completely removed by several washing steps using 2 M aqueous NaOH solution.

Pt nanoparticles incorporation onto the Co_3O_4 supports was carried out by sonication process at the 40 kHz ultrasound frequency with 80 W power output for 3 h. The nanocomposite particles were collected by centrifugation, thereafter, washed three times with ethanol and dried overnight at 353 K.

2.2. Catalytic measurements

The catalytic reactions were carried out at 1 atm pressure in a fixed-bed, continuous-flow reactor (8 mm i.d.), the temperature of which was controlled by a thermocouple. Typically, the reactor contained 200 mg of slightly compressed pellets as a catalyst and the dead volume of the reactor was filled with quartz. In the reacting gas mixture, the CO_2:H_2 molar ratio was 1:4. The reactant gas mixture CO_2:H_2 (molar ratio was

1:4) was introduced into the reactor with the total flow rate of 50 ml·min^{-1}. Agilent 4890 gas chromatograph, equipped with Equity-1 capillary and Porapak QS packed columns as well as with thermal conductivity and flame ionization detectors to assure complete separation and quantification of the gases, was used. Before the catalytic experiments, the as received catalysts were oxidized in O_2 atmosphere at 573 K for 30 min and thereafter were reduced in H_2 at 573 K for 60 min. Pre-treatment conditions were the same for all other characterization measurements unless otherwise stated.

2.3. Characterization techniques

XRD studies of the fabricated catalysts were performed on a Rigaku MiniFlex II instrument with a Ni-filtered CuK_{α} source in the range of $2\theta = 20–80°$.

For XPS analysis, samples were pre-treated in the modified pre-chamber of Kratos Analytical XSAM800 instrument and then exposed to the CO_2:H_2 gas mixture at 400 °C for 30 min. The XP spectra were obtained with a Kratos Analytical XSAM800 instrument equipped with a non-monochromatized Mg $K\alpha$ X-ray source and the X-ray gun operated at 144 W. All high-resolution spectra were charge corrected for the aliphatic component of the C1s spectrum region having peak maximum at 284.8 eV.

The temperature-programmed desorption (TPD) measurements were performed in a BELCAT-A apparatus using a reactor (quartz tube with 9 mm outer diameter) that was externally heated. Pre-treated catalysts were cooled in flowing He to 323 K and equilibrated for 15 min. The samples were flushed with CO_2 for 30 min and then flushed with He for 15 min at 323 K. The reactor was heated linearly at a rate of 10 K·min^{-1} up to 573 K. The CO_2 consumption was detected by a thermal conductivity detector (TCD).

The DRIFTS analyses were carried out in 'Agilent Cary-670' FTIR spectrometer with 'Harrick Praying Mantis' diffuse reflectance attachment. The sample was pre-treted, cooled down to room temperature under Helium flow and background spectrum was registered. At room temperature, a CO_2:H_2 mixture and He stream with total flow rate of 40 ml·min^{-1} was fed into the DRIFTS cell. The catalyst was heated linearly up to 673 K with a heating rate of 20 K·min^{-1} and IR spectra were measured at 50 K intervals.

TEM images of the samples presented on a carbon coated copper grid were provided by FEI TECNAI G2 20 X-Twin high-resolution transmission electron microscope (equipped with electron diffraction) operating at an accelerating voltage of 200 keV. For high-resolution experiments, a Cs-corrected Thermofisher Themis 200 microscope with an accelerating voltage of 200 keV was used. EDS maps were recorded using Super-X EDX detectors in STEM mode.

Co K-edge and Pt L_{III}-edge X-ray absorption fine structure (EXAFS) spectroscopy measurements were carried out at room temperature at the XAFS beamline of ELETTRA synchrotron in Trieste (Italy). The powder sample was pelletized with boron nitride. The EXAFS spectra were collected in the energy range 6.5–8.9 keV for Co K-edge in transmission mode as well as 10.3–12.7 keV for Pt L_{III}-edge in fluorescence mode. A Si (1 1 1) double-crystal monochromator was applied. The data analysis was carried out by using "EXAFSPAK" program package. The 3.0–13.0 Å data range for K^3 Fourier transform (FT) was applied, while 1.5–4.5 Å for Co and 1.4–3.5 Å for Pt distances were simulated.

3. Results and discussion

3.1. Catalytic activation in CO_2 methanation

Pt nanoparticles were loaded onto Co_3O_4 supports by the sonication process. The loaded Pt nanoparticles were well distributed all over the surface of supports with the average particle size of 4.8 ± 0.5 nm and 4.6 ± 0.9 nm for Pt/m-Co_3O_4 and Pt/c-Co_3O_4 accordingly (Fig. 1a, b). Mesoporous structure with nanorod morphology was replicated during
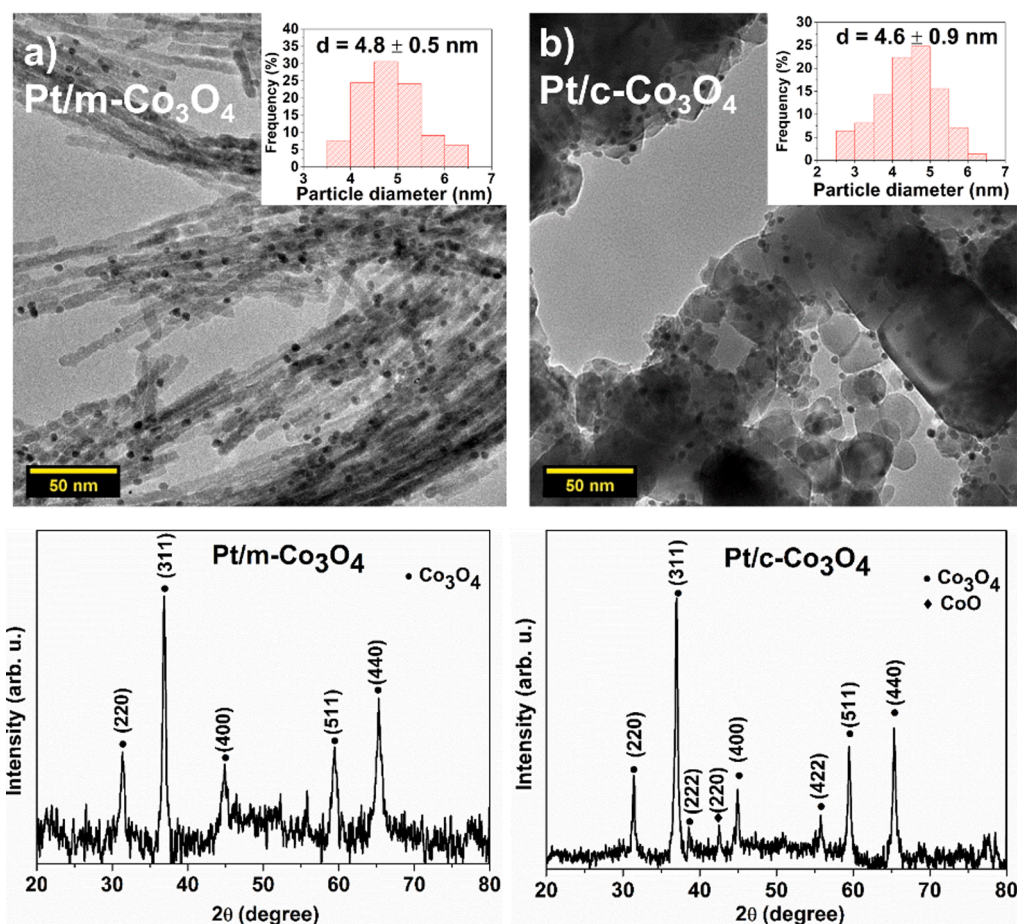
Fig. 1. Representative TEM images of Pt/m-Co₃O₄ and Pt/c-Co₃O₄ with the Pt size distribution histograms (a, b) and corresponding XRD patterns (c, d).

the preparation of m-Co₃O₄, while commercial c-Co₃O₄ was previously shown to have no ordered structure [14]. Textural properties of the supported catalysts were not significantly altered by the 1% Pt nanoparticles loading in harmony with the literature data [22] (Table S1). As-prepared catalysts were also studied with XRD to identify the sample composition. The observed peak positions are in a good agreement with the Joint Committee on Powder Diffraction Standards (JCPDS) database values. The reflections of Pt were not detected in either case due to its low loading and high dispersion. Like the pristine support, Pt/m-Co₃O₄ exhibited peaks assigned exclusively to the Co₃O₄ cubic spinel phase at 2θ = 31.3, 36.9, 44.8, 59.4, and 65.36° (JCPDS card no. 43–1003) (Fig. 1c) [14,23]. The major phase in Pt/c-Co₃O₄ was also cubic spinel Co₃O₄ with additional peaks at 2θ = 38.6 and 55.8° corresponding to the (2 2 2) and (4 2 2) crystal planes. Similar to the c-Co₃O₄, cubic CoO phase was detected in the case of Pt/c-Co₃O₄ by the most intensive reflection at 2θ = 42.5° of (2 0 0) crystal plane (JCPDS No. 43–1004) [24] (Fig. 1d).

As-prepared catalysts were subjected to the CO₂ methanation at ambient pressure in the 473 K – 673 K temperature range (Fig. S1a). As shown in Fig. 2, free-standing Co₃O₄ supports show notable catalytic performance [14], however, their activity is further improved in the entire temperature range by Pt nanoparticles loading, which comes together with the deterioration in methane selectivity (Fig. S1b). Previous studies revealed that Pt nanoparticles have weak interaction with CO₂ molecules and favour RWGS pathway, which could be an explanation for the increased CO selectivity [19,20]. On the other hand, Pt nanoparticles also aid in hydrogen spillover [25,26], thus, promoting the catalytic activity. Apart from the improvements in catalytic activity, Pt nanoparticles also contribute to the stabilization of the catalysts by slowing down their deactivation. This is particularly apparent in the case of Pt/c-Co₃O₄ (Fig. S1a, Fig. S1c). It is also perceptible that Pt

enhancement effect is bigger in the case of c-Co₃O₄ and is more pronounced with the increase in the reaction temperature. At 673 K, Pt enhancement effect represented as the CO₂ consumption rates ratios reaches ~ 1.9 times for Pt/c-Co₃O₄ whereas for Pt/m-Co₃O₄ it is ~ 1.4 (Fig. 2d). Pt enhancement effect was also calculated in terms of CH₄ selectivity and is represented as the CH₄ formation rates ratios at 673 K in the Fig. S1d.

3.2. Preliminary characterization of Pt/Co₃O₄ system

Examination of surface species present on a catalyst during a catalytic process is crucial for unravelling the reaction network. With this aim, the same way as for free-standing supports, XPS measurements were also performed and evaluated over Pt-loaded catalysts [14]. Co 2p positions and their assignments agree well with the literature findings [27,28]. The results are summarized in Table 1 and the Co 2p spectra are given in Fig. S2. Regarding the changes in the oxidation state of Co species, the same tendency was observed as for the pure supports: Pt/c-Co₃O₄ is more easily reduced by the pre-treatment process; after CO₂ hydrogenation reaction the Co²⁺ state dominates in Pt/m-Co₃O₄ catalyst (80.53%) while the Pt/c-Co₃O₄ is mostly reduced [14]. Comparing to the free-standing supports, generally the reducibility of the catalysts is improved, most probably due to the H₂-spillover effect [29,30].

It is also interesting to note that after CO₂ methanation the fraction of Cobalt oxide phase is increased compared to pure supports. Thus, c-Co₃O₄ was shown to be very prone to reduction and was 100% reduced by the reaction conditions [14] while in the Pt nanoparticles loaded sample, Cobalt oxide phase remains after CO₂ methanation with the metallic Co proportion comprising just 74.83%. This was also confirmed by the means of Temperature Programmed Oxidation (TPO), which is
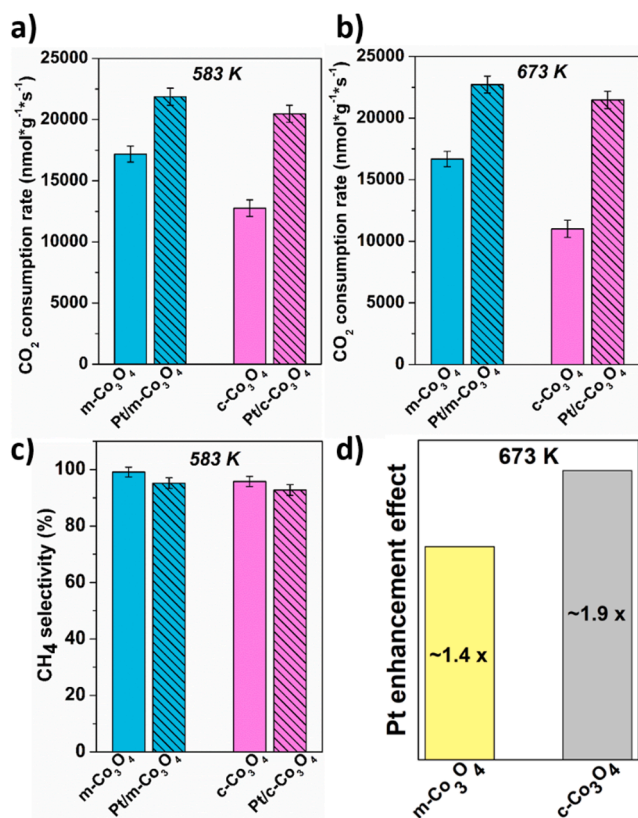
Fig. 2. CO_2 consumption rate over m-Co_3O_4, Pt/m-Co_3O_4, c-Co_3O_4, Pt/c-Co_3O_4 at 583 K (a), 673 K (b), their CH_4 selectivity at 583 K (c), and Pt enhancement effect represented as the CO_2 consumption rates ratios at 673 K (d).

Table 1

Surface atomic concentrations and ratios as determined by XPS on the pretreated and reacted catalysts.

XPS DATA				
	Co(0), %	Co(II), %	Co(III), %	O_{ads}/O_{latt}
m-Co_3O_4 pre-treated	34.20	48.10	17.70	1.22
Pt/m-Co_3O_4 pre-treated	40.97	42.25	16.78	1.99
m-Co_3O_4 reacted	24.81	68.80	6.39	
Pt/m-Co_3O_4 reacted	19.47	80.53	0.00	
c-Co_3O_4 pre-treated	46.67	54.33	0.00	1.78
Pt/c-Co_3O_4 pre-treated	54.59	45.41	0.00	1.65
c-Co_3O_4 reacted	100.00	0.00	0.00	
Pt/c-Co_3O_4 reacted	74.83	25.17	0.00	

commonly applied to study thermal oxidative behaviour of the materials (Fig. S3). Pure c-Co_3O_4 support is characterized by a broad oxygen absorption band at 353 °C, which is attributed to the oxidation of metallic cobalt to Co_3O_4 [31]. In the literature data, the absorption peak is located around 393 °C; the difference in the peak position we ascribe to the differences in the Cobalt oxidation states and structure. The shift towards lower temperature (~25 °C) for the c-Co_3O_4 after the addition of Pt signifies that Pt nanoparticles facilitate oxidation of the support. This tendency is observed to a smaller extent in the case of Pt/m-Co_3O_4 as well – the fraction of Cobalt oxide phase is increased in the spent catalyst. The oxidation of the surface of the support after addition of Pt nanoparticles in CO_2 hydrogenation reaction was reported for other systems as well, for example, for Pt/MnO_2-M200 [32].

As mentioned above, the key structural property of m-Co_3O_4 responsible for its superior activity in converting CO_2 to methane is the enhanced basicity [14]. Therefore, it seemed relevant to determine the influence of Pt nanoparticles on the catalyst basicity. CO_2-temperature-

programmed desorption (CO_2-TPD) measurements were carried out in the 323 K-573 K temperature range since weak basic sites found in this range were determined to assist CO_2 methanation [14]. Fig. S4 represents CO_2-TPD curves for thermally treated free-standing supports in comparison with their supported counterparts. Pt nanoparticles incorporation resulted in an increased sorption capacity of both catalysts to a different extent – 2.4 times in the case of Pt/m-Co_3O_4 and 4 times for the Pt/c-Co_3O_4. It should be noted that the absolute value of the number of weak basic sites was the highest for Pt/m-Co_3O_4, which may be related to the catalytic performance in the CO_2 methanation. Interestingly, Pt nanoparticles immobilization generates a new type of hydroxyl groups (dotted lines in Fig. S4) rather than enhances the already existing ones. Moreover, for Pt/c-Co_3O_4 the increase in the peak area was also accompanied by the shifting in the peak position to higher temperatures indicating a stronger CO_2 affinity of the Pt/c-Co_3O_4 catalyst.

3.3. Reaction mechanism discussion

Identification of surface adsorbed species is essential in establishing the mechanism of heterogeneously catalysed reaction. Towards this goal, DRIFTS spectra were collected at elevated temperatures in the presence of the reactant mixture/products on both the samples (Fig. 3). It should be noted that the denoted wavenumbers may vary by ± 5 cm^{-1} within one data set as a function of temperature. The observed bands formed during CO_2 methanation and assigned to them adsorbed species are listed in Table S2.

In the spectra of Pt/m-Co_3O_4 (Fig. 3a), two strong twin-bands at 3750–3550 cm^{-1} belong to the combined tones of gas and adsorbed CO_2 molecules [33] and indicate high CO_2 adsorption due to the increased number of weak basic sites as shown by CO_2-TPD results. The formation of the main product – methane – is detectable at 1305 cm^{-1} and 3016 cm^{-1} from 473 K as in the case of free-standing m-Co_3O_4 [14]. The assignment of observed IR bands was carried out based on the assignment proposed previously for pure Co_3O_4 supports [14] as well as on the publications reporting the formation of relevant surface species under similar conditions mentioned below.

During CO_2 methanation among other peaks, two bands develop at room temperature positioned at 1645 cm^{-1} and 1215 cm^{-1} which afterwards simultaneously completely disappear at 423 K. Those vibrational modes were assigned to bicarbonate species generated by the interactions of CO_2 with the weak basic sites – surface hydroxyls [34,35]. From 423 K bicarbonate species are transformed to formate species at 2848 cm^{-1}, 1575 cm^{-1}, and 1376 cm^{-1} [14]. The formate intermediate was reported to play an important role in the CO_2 methanation [35–40]. The formate species can be hydrogenated to hydrocarbons:

$$HCOO_{(a)} \rightarrow H_2COH_{(a)} \rightarrow H_2C_{(a)} + OH_{(a)} \tag{1}$$

$$H_2C_{(a)} + 2H_{(a)} \rightarrow CH_{4(g)} \tag{2}$$
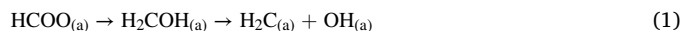
Moreover, a broad peak at 1970 cm^{-1} is detected from 373 K. This band is assigned to the bridge bonded or hydrogen-perturbed CO species, which could emerge from formate species [37,38,41].

Apart from formate pathway, methane formation additionally occurs through the RWGS mechanism in the case of Pt/m-Co_3O_4 as well. This is apparent from the small intensity linearly adsorbed CO peak at 2076 cm^{-1}, which shifts to lower wavenumbers upon increasing the temperature. Its appearance at low temperatures indicates that CO_2 may undergo dissociative adsorption on the surface of Pt/m-Co_3O_4:

$$CO_{2(g)} \rightarrow CO_{(a)} + O_{(a)} \tag{3}$$

At high temperatures, CO selectivity is considerably increased. Gaseous CO may originate from the decomposition of formate species:
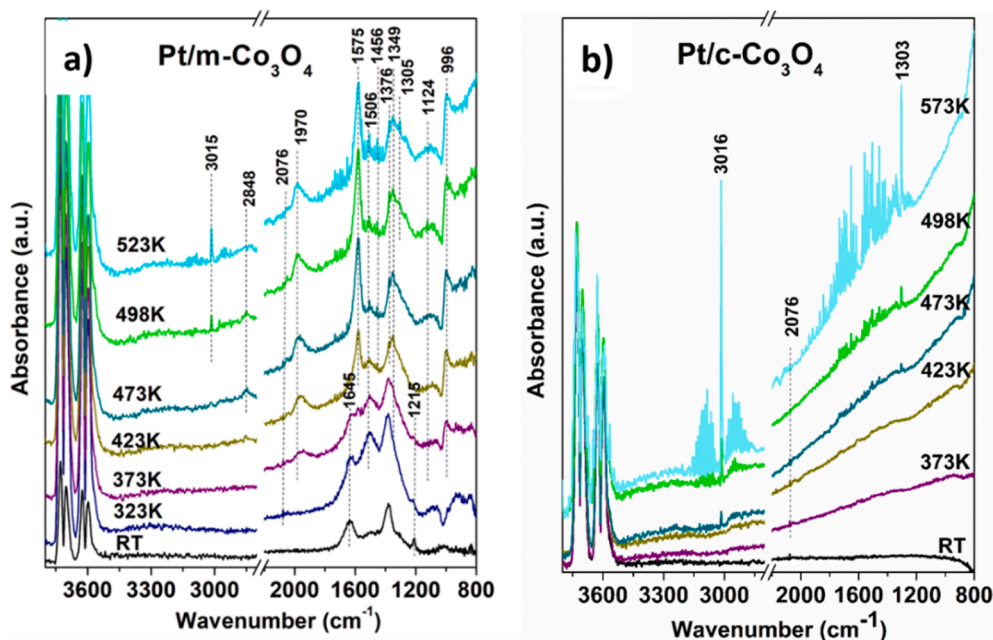
$$HCOO_{(a)} \rightarrow CO_{(a)} + OH_{(a)} \tag{4}$$

Fig. 3. In-situ DRIFTS spectra of Pt/m-Co$_3$O$_4$ (a) and Pt/c-Co$_3$O$_4$ (b) obtained during CO$_2$ hydrogenation.

This reaction step (eq. (4)) was considered recently in CO$_2$ + H$_2$ reaction in several cases, for example on NiO, Pt/NiO [37], on Ru/Al$_2$O$_3$ [36], on Au/TiO$_2$ [42] on Co/MnO$_x$ [41] Furthermore, formate produced by adsorption of HCOOH on metals [43], on oxide and supported metal catalysts [44,45] decomposes to CO and CO$_2$.

Besides reactive intermediates, several types of carbonate species were also distinguished in the case of Pt/m-Co$_3$O$_4$. Bands at 1506 cm^{-1}, 1349 cm^{-1}, 993 cm^{-1} are referred to the monodentate form of carbonate species [14,46,47] while those at 1456 cm^{-1} and 1124 cm^{-1} belong to polydentate carbonate species [14,48].

In the case of Pt/c-Co$_3$O$_4$ catalyst, the reaction is initiated at 473 K revealed by the appearance of the methane related bands at 1305 cm^{-1} and 3016 cm^{-1} (Fig. 3b). It is noteworthy, that CO$_2$ adsorption is significantly enhanced in this case as opposed to non-loaded c-Co$_3$O$_4$ support, which is reflected in the emergence of two twin-bands at 3750–3550 cm^{-1}. For the c-Co$_3$O$_4$, these bands in the corresponding spectral region were completely missing [14]. This is justified by the substantial grow of weak basic sites (x 4 times more on Pt/c-Co$_3$O$_4$ as shown by the CO$_2$-TPD data), which greatly assists in CO$_2$ adsorption and hence improves its subsequent conversion.

Major surface species detected for Pt/c-Co$_3$O$_4$ were linearly adsorbed CO molecules which appeared at 2076 cm^{-1}. The formation of adsorbed CO takes place through RWGS mechanism according to the equation (3). Even though no other intermediates with considerable concentration could be identified, the increase in the weak basic sites implies that hydroxyl groups are present on the surface. The enhanced CO$_2$ adsorption most likely originates from the interaction of surface OH groups and the CO$_2$ molecules with the formation of bicarbonate species. Contrary to the free-standing c-Co$_3$O$_4$, the formate pathway cannot be excluded for the Pt/c-Co$_3$O$_4$ since formate intermediate is able to accumulate on the oxide surface [49].

The possibility of carbon route, in which subsurface carbon is hydrogenated to methane, was also considered. This mechanism was established to operate on a Cobalt Fischer–Tropsch catalyst [50]. To investigate the validity of this reaction pathway in the case of Pt/c-Co$_3$O$_4$ catalyst, switching experiments were conducted (Fig. 4). Firstly, reaction gas mixture (CO$_2$ + H$_2$) was introduced to the pre-treated catalyst at 498 K. The course of the reaction was monitored by following the bands at 1303 cm^{-1} and 3016 cm^{-1} the appearance of which indicates methane formation. Once the reaction is initiated,
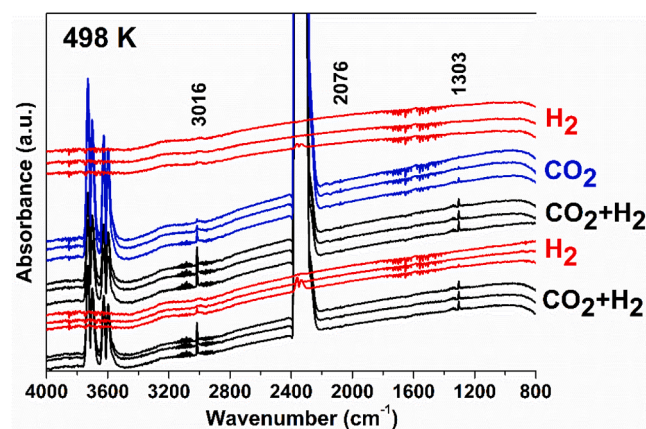

Fig. 4. In-situ DRIFTS spectra obtained by performing following switches over the pre-treated Pt/c-Co$_3$O$_4$ at 498 K: CO$_2$ + H$_2$ reactant gas mixture exposure; only H$_2$ flow exposure (CO$_2$ flow removed); only CO$_2$ flow exposure (H$_2$ flow removed) for 1, 5 and 25 min.

linearly adsorbed CO peak at 2076 cm^{-1} also emerges. Then the CO$_2$ flow was eliminated and only the hydrogen flow was let to the surface. If deposited carbon was active and could be converted to methane, the methane formation would occur even in the absence of the carbon source. However, the corresponding methane features were not detected. The reactant gas mixture was afterwards introduced again, and the intense methane formation was observed. When the H$_2$ flow was removed, methane formation quietened. Repeated exposure of the surface to the H$_2$ stream did not result in the formation of methane, which implies that no accumulation of active carbon occurs. Overall, it can be concluded that for Pt/c-Co$_3$O$_4$ only RWGS mechanism was proven to provide catalytic activity, nevertheless, the participation of formate species to produce methane cannot be ruled out.

Interestingly, carboxylate pathway was established for both free-standing Co$_3$O$_4$s supports, however, no carboxylate species were observed on Pt nanoparticles supported samples. It was also suggested that carboxylate intermediate is stabilized by oxygen vacancies dominating on the c-Co$_3$O$_4$ [14]. For supported catalysts we propose that the

oxygen vacancies are favourable sites for Pt nanoparticles positioning as it was calculated for Pt clusters/defective anatase surface [51]. To this end, the same way as for pure Co_3O_4 samples, the ratio O_{ads}/O_{latt} was calculated for supported samples (Table 1), where the peak located at ~531 eV corresponds to surface adsorbed hydroxyl species (O_{ads}) and peak at ~529 eV is assigned to lattice oxygen species (O_{latt}). The ratio itself provides an insight into the number of surface oxygen vacancies: higher ratio indicates more oxygen vacancies. Change in the ratio after Pt nanoparticles loading may be associated with two factors: increase in the weak basic sites – hydroxyl species – and decrease in oxygen vacancies sites. For m-Co_3O_4 value of 1.22 was reported which with the incorporation of Pt nanoparticles has increased to 1.99. The increase in the value maybe mainly attributed to the increase in weak basic sites, since the number of oxygen vacancies was not significant in this case. In the case of Pt/c-Co_3O_4, the value slightly dropped from 1.78 to 1.65. The decrease of the value denotes the decrease in the number of oxygen vacancies, and this consequently can serve as an indirect proof that Pt nanoparticles are preferably positioned in V_O sites.

The main route for carbon formation observed by TEM in both the cases is suggested to be the direct C-O bond cleavage in adsorbed CO:

$$CO_{(a)} \rightarrow C_{(a)} + H_{(a)} \qquad (5)$$
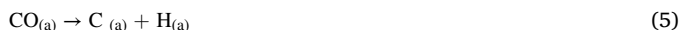
3.4. Discussion on the active sites and characterization of spent catalysts

In the catalytic systems comprised of the noble metals supported mesoporous metal oxides, noble metals or noble metal/metal oxide interphase are most commonly referred as active sites in the CO_2 hydrogenation reaction [52,49,53]. It is well known that CO readily adsorbs on Pt sites [54]. Moreover, CO adsorption does not occur on Co_3O_4 surface above room temperature [55]. Therefore, carbon monoxide chemisorption can provide a powerful surface sensitive technique to investigate surface structure changes of Pt nanoparticles. Carbon monoxide was firstly adsorbed on thermally treated Pt/Co_3O_4 catalysts (pretreatment process includes oxidation with subsequent reduction at 573 K) at RT and after He flush was subjected to programmed heating similar to the CO_2 methanation conditions (Fig. S5). In the 2200–2000 cm^{-1} wavenumber range, in which linearly adsorbed CO is expected to appear, no peak was detected [55] (Fig. S5). To track the formation of Pt nanoparticles in each case, more detailed CO chemisorption analysis was carried out (Fig. 5). Here, both Pt/Co_3O_4 samples were firstly

oxidized at 573 K, flushed with Helium, and subjected to the CO adsorption at room temperature (RT) (Fig. 5). The reported spectra show a strong band at 2094 cm^{-1} resistant to He flushing which corresponds to Pt^{2+}–CO species [54]. Then the CO was introduced at different reduction temperatures. In both the cases, the chemisorbed CO band remains stable with the increase of the reduction temperature, which is accompanied by the considerable decrease in intensity. The band visibly disappears after the reduction at 573 K, however, zooming in allows to register a small intensity adsorbed CO peak (Fig. 5a Inset, 5b Inset). The smaller availability of Pt sites for the CO adsorption can designate a common feature of surface processes including encapsulation and formation of a core–shell structure in which during reductive treatment the particles are covered by other lower surface energy islets, however, they recover under reoxidation [56,57]. It may be speculated that under the reductive treatment, a reconstruction of the surface occurs, which leads to the Pt nanoparticles being covered by Co_xO_y overlayer like in the Pt/CeO_2 case [58].

The increased strength of basic sites shown by CO_2-TPD results and migration of Pt nanoparticles from the surface shown by CO_2 chemisorption analysis suggest that some structural changes occur to the catalysts during the CO_2 methanation. Therefore, investigation of catalysts' structures in spent samples containing 1% 5 nm Pt on Co_3O_4 particles was performed with High-Resolution Transmission Electron Microscopy (HR-TEM) along with High-angle annular dark-field scanning transmission electron microscopy (HAADF-STEM) and Energy Dispersive X-Ray Spectroscopy (EDS).

Fig. 6. represents the typical result for the spent Pt/m-Co_3O_4. Elongated crystalline carbon nanofibers were observed, at the end of which Co-containing particles were located in the size of 10–50 nm (Fig. 6a). Based on HAADF STEM and EDS studies, Platinum was dissolved in Co-containing particles (Fig. 6b, 6c, 6d). The majority of Co-containing particles show the presence of Platinum. However, due to the low Platinum content, in some places of the EDS map it was visible on the carbon membrane as an artefact. (Fig. 6d red square). These areas were dark in the HAADF image, so the presence of unique Platinum grains is excluded.

In the case of Pt/c-Co_3O_4, a few nm amorphous carbon layer was detected on the surface of Pt/c-Co_3O_4. Most of the Co-containing particles were larger than 100 nm in size. The EDS mapping images reveal the presence of the overlapped matrix between Co and Pt, in which Pt forms crystals of a few nm that are directed to the surface of the large Co particles (Fig. 7b, 7c). Pt crystal phase could not be clearly identified,
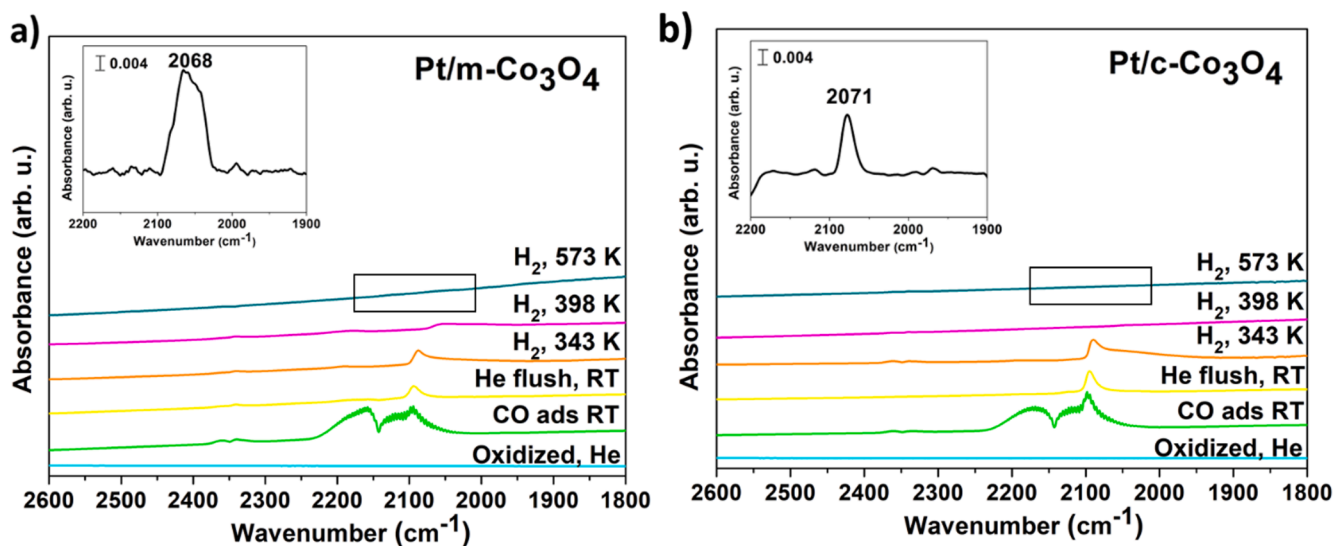

Fig. 5. CO chemisorption analysis. IR spectra of Pt/m-Co_3O_4 (a) and the Pt/c-Co_3O_4 (b) obtained during CO adsorption over oxidized catalysts at different conditions. Inset: zoomed black square region of Pt/m-Co_3O_4 (a) and Pt/c-Co_3O_4 (b).
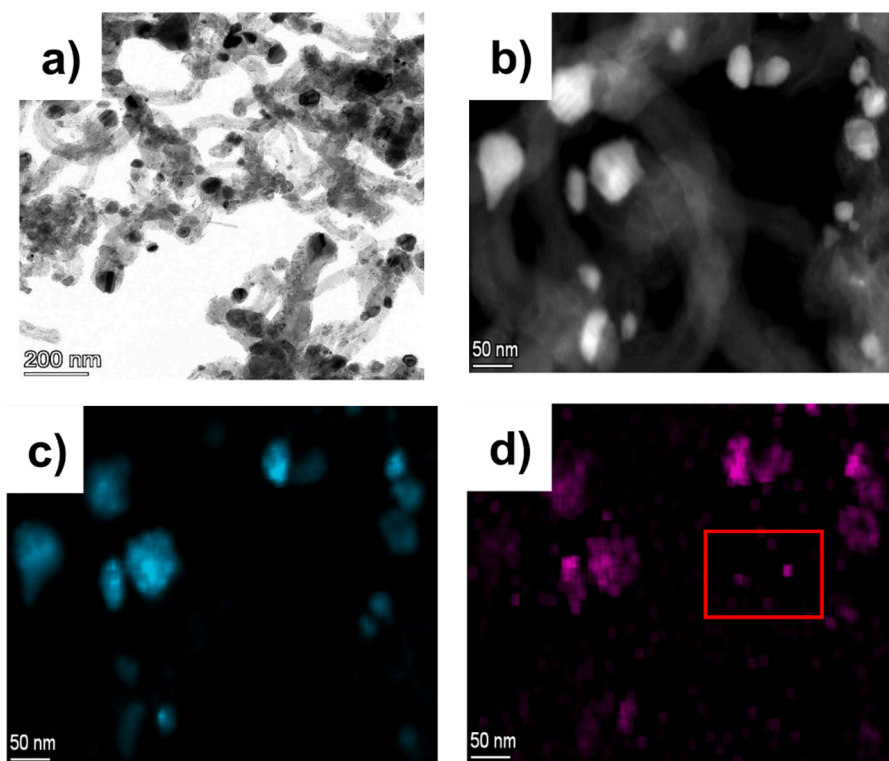
Fig. 6. Representative TEM image (a); HAADF STEM image (b); EDS elemental maps of Co (c); and Pt (d) of spent Pt/m-Co$_3$O$_4$.
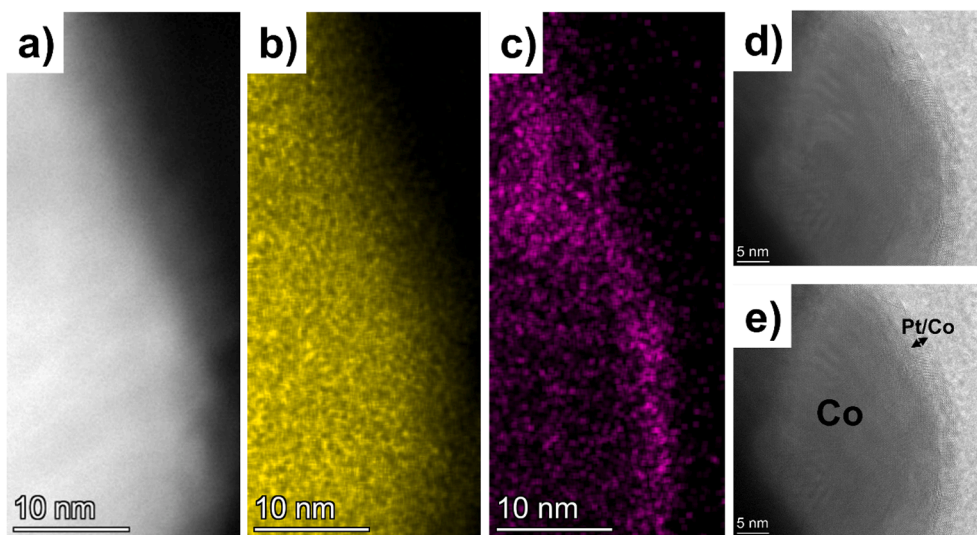

Fig. 7. HR-TEM image (a); marked HR-TEM image (b); HAADF STEM image (c); EDS elemental maps of Co (d); and Pt (e) of spent Pt/c-Co$_3$O$_4$.

most likely because it is alloyed with Co. The formation of Co-Pt alloy layer on large Co-containing particles is shown in the Fig. 7d, 7e.

Altogether, the formation of structured carbon on mesoporous Co$_3$O$_4$ and amorphous carbon on bulk Co$_3$O$_4$ (in our case bulk morphology is very close to the morphology of c-Co$_3$O$_4$) after CO$_2$ hydrogenation reaction was shown previously for free-standing supports [59]. The EDS results suggest the alloy formation for both Pt/c-Co$_3$O$_4$ and Pt/m-Co$_3$O$_4$. Formation of a Co-Pt alloy can additionally be supported by such complementary technique as XPS. However, the deconvolution of Pt 4f XPS spectra of the catalysts after pre-treatment has led to ambiguous results. To confirm the formation of alloyed structure as well as to characterize the oxidation states and coordination environments of Co in the Pt/m-Co$_3$O$_4$, X-ray absorption fine structure (EXAFS) spectra were recorded.

EXAFS spectra were fitted in order to evaluate data on the Co K-edge (Fig. S6a). The spectra contain Co–O with interatomic distance centred in 2.05 Å and coordination number of 5.7 (Table 2), indicating the dominant presence of Co(II)–O (octahedral) species. The fitted data coincide well with those of Co(II)-O bonds in CoO or Co$_3$O$_4$ compounds [31,60]. In addition, other Co–O distances in the first coordination sphere of the cobalt were verified. The identified modulus was shifted towards the longer interatomic distances (2.27 Å) and belongs to the Co(III)–O (tetrahedral) species with average coordination number of 3.1. X-ray absorption spectra (XAS) data, which clearly showed the appearance of the Co(II)–Co(III) or Co(II)–Co(II) interatomic distances with coordination number of 3.8, are similar to those of the neighbouring shells of the Co$_3$O$_4$ compounds [31]. Further quantitative

Table 2
EXAFS data on the metal (ions) in the spent Pt/m-Co$_3$O$_4$.

EXAFS data on the Co K-edge Fitted interatomic distances	N_{M-X}	R_{M-X} (Å)	σ^2 (Å^2)	E_0 (eV)	F-factor
Co(II)–O (octahedral)	5.7	2.05	0.0012	–2.5511	19.53% (total: 24.12%)
Co(III)–O (tetrahedral)	3.1	2.27	0.0045	–5.6414	
Co(0)–Co(0)	7.7	2.58	0.0050	0	
Co(II)–Co(II/III)	3.8	3.35	0.0160	–3.8200	
Co(II)–O	22.8	3.59	0.0250	–5.6011	
EXAFS data on the Pt L$_{III}$-edge					
Pt(IV)–O (octahedral)	4.1	2.08	0.0011	–2.1302	18.35% (total: 34.10%)
Pt(0)–Pt(0)	11.1	2.98	0.0350	0	
Pt(0)–Co(0)	5.9	2.52	0.0230	1.7100	
Pt(IV)–O	23.0	3.48	0.0350	–2.0914	

analysis revealed that there is a Co–Co bonding in the spent Pt/m-Co$_3$O$_4$ [28]. The simulations also exhibited a significant decrease in N_{Co-Co} compared to the reference metallic Co, which represents a similar phenomenon as in the case of the previously studied cobalt(-oxide) supported noble metal systems, and indirectly indicates the possibility of an alloy formation [61].

On the basis of the evaluation of the measured EXAFS oscillations on Pt L$_{III}$-edge (Fig. S6b), having average coordination number of 11.1, it was possible to identify a Pt–Pt distance centred in 2.98 Å (Table 2). There is no-reacted metallic Platinum compound in the composite after the catalytic reaction [62]. The scattering of the catalyst in the high coordination spheres are related to the modulus of FCC Platinum. To evaluate the measured data, interatomic distance of 2.08 Å with octahedral sphere in the first coordination shell is considered. This distance is assigned to the Pt(IV)–O bonding which demonstrates the partial oxidation of the Pt nanoparticles [63]. Additionally, the presence of Pt–Co heteroatomic bonds in the spent catalyst was detected [64]. Considering the previously studied linearly correlations about the compositions and interatomic distances in Pt-Co alloys (Vegard's law), the 9:1 of Co:Pt actual molar ratio could be given for alloy by calculating 2.52 Å distance which is very similar to that of values reported [28,65,66].

XAFS results have verified the presence of Co(0)-, Co(II)-oxide- and Co(III)-oxide-containing species as well as the formation of Co$_9$-Pt$_1$ alloy in the spent Pt/m-Co$_3$O$_4$ sample. Even though the Pt–Pt bond was registered, TEM (-EDX) analysis results clearly exclude the presence of free Pt nanoparticles on the surface. Therefore, invidual Pt nanoparticles are assumed to remain in the bulk of the catalyst.

On the whole, Co-Pt alloy with high Co content maybe suggested in both cases. By the means of the CO$_2$-TPD analysis, it was found that Pt nanoparticles incorporation increased the number of weak basic sites, more significantly for the Pt/c-Co$_3$O$_4$ (Fig. S4). This was also reflected in the increased CO$_2$ adsorption shown by the DRIFTS spectra (Fig. 3). Based on the literature data, formation of Pt-Co itself is not responsible for the basicity alteration. In turn, hydroxyl groups can exist on an oxide surface [67]. From Fig. S4 it is also observable that Pt nanoparticles incorporation results in the generation of a new, same for both catalysts, type of hydroxyl groups. Considering this, a different type of Cobalt Oxide – Co$_x$O$_y$ – was involved in the basicity improvement. We propose that Co-Pt alloy particles were partially covered by the Co$_x$O$_y$ overlayer as it was suggested from the CO chemisorption analysis results. Alloying with Cobalt can increase Platinum surface energy [68] and enable the Co-Pt alloy to be covered by Co$_x$O$_y$. This structure reconstruction process may be responsible for the creating energy favourable sites for the adsorption of water, thus, generating surface hydroxyl groups and increasing basicity. Discussing the matter, it can be easily spotted that higher basicity enhancement in the case of Pt/c-Co$_3$O$_4$ did not lead to the best catalytic performance. In this regard, we must suggest that the

beneficial impact of the basicity increase onto the catalytic activity manifests itself not in a linear fashion but reaches some saturation.

Unlike free-standing support, which was completely reduced during the reaction, Pt/c-Co$_3$O$_4$ showed some CoO on the surface. This oxidation is suggested to happen around partially covered Co-Pt alloy particles. For Pt/m-Co$_3$O$_4$, Cobalt oxide was dominating with smaller proportion of metallic Co. Hence, partially covered by Co$_x$O$_y$ overlayer Co-Pt alloy particles are represented to be dissolved in CoO. Formate species stemmed from the interaction of carbon dioxide with weak basic sites were additionally generated on the Pt/m-Co$_3$O$_4$ catalyst. Normalizing the amount of emerged with the Pt incorporation hydroxyl groups to the BET surface area, it can be determined that more active centres are located on the Pt/c-Co$_3$O$_4$, which explains the higher enhancement effect of Platinum in the catalytic activity in this case.

Combining HR-TEM (-EDX), EXAFS, XPS, CO$_2$-TPD, DRIFTS data and the results of the CO chemisorption analysis, we propose the following sketch (Fig. 8.), illustrating the structure and mechanisms operating for the catalysts during CO$_2$ methanation reaction.

4. Conclusions

The incorporation of 1% 5 nm Pt nanoparticles onto m-Co$_3$O$_4$ and c-Co$_3$O$_4$ allowed higher CO$_2$ consumption rates, slightly diminishing their CH$_4$ selectivity in the CO$_2$ hydrogenation reaction. The catalytic activity enhancement effect was more significant in the case of Pt/c-Co$_3$O$_4$, and it was accompanied by the more pronounced increase in the number of weak basic sites. By the means of XPS, it was found out that after pretreatment, Pt nanoparticles facilitate the reduction of the catalysts through H$_2$-spillover, however, after CO$_2$ methanation, the oxidation of the catalysts is improved. HR-TEM, EDX and EXAFS results suggest the Co-Pt alloy formation in both cases. From the carbon monoxide chemisorption analysis, it was discovered that during the reductive pretreatment Co-Pt alloy particles are partially covered by Co$_x$O$_y$ overlayer. It has been speculated that this structure rearrangement creates new basic centres. Thus, Pt/c-Co$_3$O$_4$ with abundant weak basic sites demonstrated great CO$_2$ capture capacity far exceeding that of the c-Co$_3$O$_4$, which resulted in the larger catalytic activity enhancement effect. While RWGS pathway was the only one proven to operate in the case of Pt/c-Co$_3$O$_4$, in the case of Pt/m-Co$_3$O$_4$, formate intermediate additionally contributes to the CO$_2$ conversion, thus, the activity of Pt/m-Co$_3$O$_4$ is the best. Unlike the free-standing supports, carboxylate route was not established for Pt-loaded catalysts, presumably due to the fact that oxygen vacancies stabilizing the carboxylate species are favourable sites for Pt nanoparticles. In present study, we pointed out that the combination of bulk- and surface-sensitive techniques provides a useful insight into the nature of metal-support surface interactions in the Pt/Co$_3$O$_4$ system. The obtained information is crucial for the elucidating of structure-catalytic activity correlations, which aids the design of active centres with desired characteristics for important industrial processes.

CRediT authorship contribution statement

Anastasiia Efremova: Conceptualization, Writing – original draft, Visualization. **Imre Szenti:** Conceptualization, Writing – original draft, Visualization. **János Kiss:** Conceptualization, Writing – review & editing. **Ákos Szamosvölgyi:** Investigation, Validation. **András Sápi:** Supervision, Project administration. **Kornélia Baán:** Investigation, Validation. **Luca Olivi:** Investigation, Validation. **Gábor Varga:** Investigation, Validation. **Zsolt Fogarassy:** Investigation, Validation. **Béla Pécz:** Investigation, Validation. **Ákos Kukovecz:** Funding acquisition, Resources. **Zoltán Kónya:** Funding acquisition, Resources.

Declaration of Competing Interest

The authors declare that they have no known competing financial interests or personal relationships that could have appeared to influence
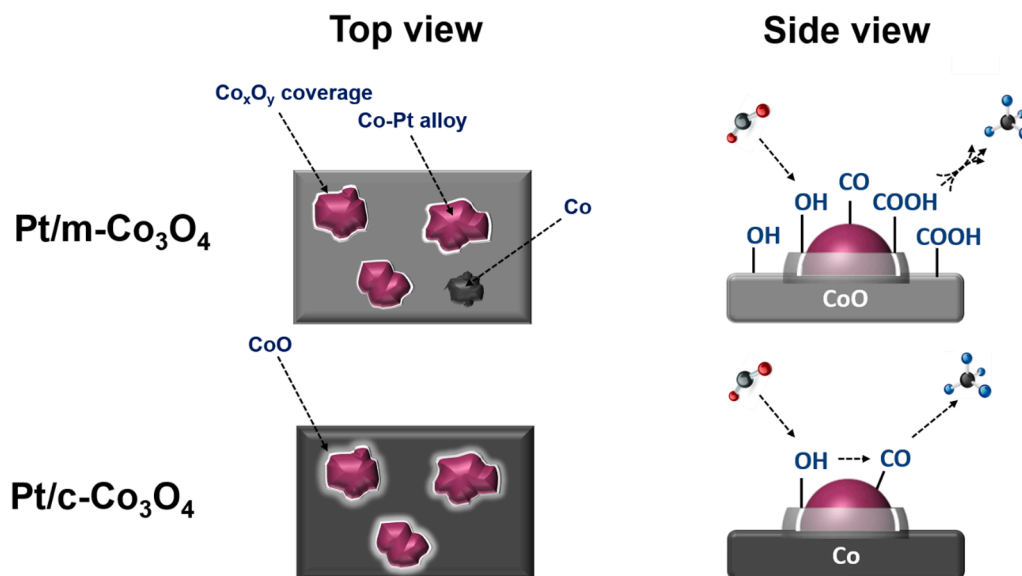
Fig. 8. Proposed structure operating during CO_2 methanation reaction on the Pt/m-Co_3O_4 and Pt/c-Co_3O_4.

the work reported in this paper.

Acknowledgement

AS gratefully acknowledges the support of the Bolyai Janos Research Fellowship of the Hungarian Academy of Science and the "UNKP-20-5-SZTE-663" New National Excellence Program of the Ministry for Innovation and Technology. ISZ is grateful for the fund of "UNKP-20-4-SZTE-634" New National Excellence Program of the Ministry for Innovation and Technology. KZ is grateful for the fund of NKFIH - OTKA - SNN 135918. The financial support of the Hungarian National Research, Development, and Innovation Office through the GINOP-2.3.2-15-2016-00013 project "Intelligent materials based on functional surfaces - from syntheses to applications" and the Ministry of Human Capacities through the EFOP-3.6.1-16-2016-00014 project and the 20391-3/2018/FEKUSTRAT are acknowledged. The access to the microscope facility is provided via the VEKOP-2.3.3-15-2016-00002 project of the European Structural and Investment Funds. The XAFS beamline of Elettra is greatly acknowledged for allowing the XAS measurements.

Appendix A. Supplementary data

Supplementary data to this article can be found online at https://doi.org/10.1016/j.apsusc.2021.151326.

References

[1] W. Wang, S. Wang, X. Ma, J. Gong, Recent advances in catalytic hydrogenation of carbon dioxide, Chem. Soc. Rev. 40 (2011) 3703–3727, https://doi.org/10.1039/c1cs15008a.

[2] W. Li, H. Wang, X. Jiang, J. Zhu, Z. Liu, X. Guo, C. Song, A short review of recent advances in CO_2 hydrogenation to hydrocarbons over heterogeneous catalysts, RSC Adv. 8 (2018) 7651–7669, https://doi.org/10.1039/C7RA13546G.

[3] T. Sakakura, J.-C. Choi, H. Yasuda, Transformation of carbon dioxide, Chem. Rev. 107 (2007) 2365–2387, https://doi.org/10.1021/cr068357u.

[4] J. Kiss, Á. Kukovecz, Z. Kónya, Beyond nanoparticles: the role of sub-nanosized metal species in heterogeneous catalysis, Catal. Lett. 149 (2019) 1441–1454, https://doi.org/10.1007/s10562-019-02734-6.

[5] B. Endrődi, A. Samu, E. Kecsenovity, T. Halmágyi, D. Sebők, C. Janáky, Operando cathode activation with alkali metal cations for high current density operation of water-fed zero-gap carbon dioxide electrolysers, Nat. Energy. 6 (2021) 439–448, https://doi.org/10.1038/s41560-021-00813-w.

[6] I. Sreedhar, Y. Varun, S.A. Singh, A. Venugopal, B.M. Reddy, Developmental trends in CO_2 methanation using various catalysts, Catal. Sci. Technol. 9 (2019) 4478–4504, https://doi.org/10.1039/C9CY01234F.

[7] W. Li, X. Nie, X. Jiang, A. Zhang, F. Ding, M. Liu, Z. Liu, X. Guo, C. Song, ZrO_2 support imparts superior activity and stability of Co catalysts for CO_2 methanation, Appl. Catal. B Environ. 220 (2018) 397–408, https://doi.org/10.1016/j.apcatb.2017.08.048.

[8] W. Li, Y. Liu, M. Mu, F. Ding, Z. Liu, X. Guo, C. Song, Organic acid-assisted preparation of highly dispersed Co/ZrO_2 catalysts with superior activity for CO_2 methanation, Appl. Catal. B Environ. 254 (2019) 531–540, https://doi.org/10.1016/j.apcatb.2019.05.028.

[9] C. Yang, S. Liu, Y. Wang, J. Song, G. Wang, S. Wang, Z.-J. Zhao, R. Mu, J. Gong, The interplay between structure and product selectivity of CO_2 hydrogenation, Angew. Chem. Int. Ed. 58 (2019) 11242–11247, https://doi.org/10.1002/anie.201904649.

[10] S. Kattel, W. Yu, X. Yang, B. Yan, Y. Huang, W. Wan, P. Liu, J.G. Chen, CO_2 hydrogenation over oxide-supported PtCo Catalysts: The role of the oxide support in determining the product selectivity, Angew. Chem. Int. Ed. 55 (2016) 7968–7973, https://doi.org/10.1002/anie.201601661.

[11] L. Wang, E. Guan, Y. Wang, L. Wang, Z. Gong, Y. Cui, X. Meng, B.C. Gates, F. S. Xiao, Silica accelerates the selective hydrogenation of CO_2 to methanol on cobalt catalysts, Nat. Commun. 11 (2020) 1–9, https://doi.org/10.1038/s41467-020-14817-9.

[12] K.Y. Kim, H. Lee, W.Y. Noh, J. Shin, S.J. Han, S.K. Kim, K. An, J.S. Lee, Cobalt ferrite nanoparticles to form a catalytic Co-Fe alloy carbide phase for selective CO_2 hydrogenation to light olefins, ACS Catal. 10 (2020) 8660–8671, https://doi.org/10.1021/acscatal.0c01417.

[13] F. Solymosi, A. Erdöhelyi, T. Bánsági, Methanation of CO_2 on supported rhodium catalyst, J. Catal. 68 (1981) 371–382, https://doi.org/10.1016/0021-9517(81)90106-8.

[14] A. Efremova, T. Rajkumar, Á. Szamosvölgyi, A. Sápi, K. Baán, I. Szenti, J. Gómez-Pérez, G. Varga, J. Kiss, G. Halasi, Á. Kukovecz, Z. Kónya, Complexity of a Co_3O_4 system under ambient-pressure CO_2 methanation: influence of bulk and surface properties on the catalytic performance, J. Phys. Chem. C. 125 (2021) 7130–7141, https://doi.org/10.1021/acs.jpcc.0c09717.

[15] J.D. Jimenez, C. Wen, M.M. Royko, A.J. Kropf, C. Segre, J. Lauterbach, Influence of coordination environment of anchored single-site cobalt catalyst on CO_2 hydrogenation, Chem. Cat. Chem. 12 (2020) 846–854, https://doi.org/10.1002/cctc.201901676.

[16] O. Brummel, Y. Lykhach, M. Vorokhta, B. Šmíd, C. Stumm, F. Faisal, T. Skála, N. Tsud, A. Neitzel, K. Beranová, K.C. Prince, V. Matolín, J. Libuda, Redox behavior of Pt/Co_3O_4 (111) model electrocatalyst studied by X-ray photoelectron spectroscopy coupled with an electrochemical cell, J. Phys. Chem. C. 123 (2019) 8746–8758, https://doi.org/10.1021/acs.jpcc.8b08890.

[17] Y. Lykhach, S. Piccinin, T. Skála, M. Bertram, N. Tsud, O. Brummel, M. Farnesi Camellone, K. Beranová, S. Fabris, K.C. Prince, V. Matolín, J. Libuda, Quantitative analysis of the oxidation state of cobalt oxides by resonant photoemission spectroscopy, J. Phys. Chem. Lett. 10 (2019) 6129–6136, https://doi.org/10.1021/acs.jpclett.9b02398.

[18] E. Gioria, L. Duarte-Correa, N. Bashiri, W. Hetaba, R. Schomaecker, A. Thomas, Rational design of tandem catalysts using a core-shell structure approach, Nanoscale Adv. 3 (2021) 3454–3459, https://doi.org/10.1039/D1NA00310K.

[19] S. Kattel, B. Yan, J.G. Chen, P. Liu, CO_2 hydrogenation on Pt, Pt/SiO_2 and Pt/TiO_2: Importance of synergy between Pt and oxide support, J. Catal. 343 (2016) 115–126, https://doi.org/10.1016/j.jcat.2015.12.019.

[20] A. Sápi, U. Kashaboina, K.B. Ábrahámné, J.F. Gómez-Pérez, I. Szenti, G. Halasi, J. Kiss, B. Nagy, T. Varga, Á. Kukovecz, Z. Kónya, Synergetic of Pt nanoparticles and H-ZSM-5 zeolites for efficient CO_2 activation: Role of interfacial sites in high activity, Front. Mater. 6 (2019) 1–12, https://doi.org/10.3389/fmats.2019.00127.

[21] F. Kleitz, S.H. Choi, R. Ryoo, Cubic Ia3d large mesoporous silica: Synthesis and replication to platinum nanowires, carbon nanorods and carbon nanotubes, Chem. Commun. 3 (2003) 2136–2137, https://doi.org/10.1039/b306504a.

[22] Q. Wang, J. Liu, Y. Li, Z. Zhao, W. Song, Y. Wei, Mesoporous Co_3O_4 supported Pt catalysts for low-temperature oxidation of acetylene, RSC Adv. 7 (2017) 18592–18600, https://doi.org/10.1039/C7RA02266B.

[23] J. Qiu, M. Yu, Z. Zhang, X. Cai, G. Guo, Synthesis of Co_3O_4/nitrogen-doped carbon composite from metal-organic framework as anode for Li-ion battery, J. Alloys Compd. 775 (2019) 366–371, https://doi.org/10.1016/j.jallcom.2018.10.129.

[24] Z. Li, D. Wu, Y. Ouyang, H. Wu, M. Jiang, F. Wang, L.Y. Zhang, Synthesis of hollow cobalt phosphide nanocrystals with ultrathin shells anchored on reduced graphene oxide as an electrocatalyst toward hydrogen evolution, Appl. Surf. Sci. 506 (2020), 144975, https://doi.org/10.1016/j.apsusc.2019.144975.

[25] C. Spreafico, W. Karim, Y. Ekinci, J.A. van Bokhoven, J. VandeVondele, Hydrogen adsorption on nanosized platinum and dynamics of spillover onto alumina and titania, J. Phys. Chem. C 121 (2017) 17862–17872, https://doi.org/10.1021/acs.jpcc.7b03733.

[26] J. Zhang, Z. Gao, S. Wang, G. Wang, X. Gao, B. Zhang, S. Xing, S. Zhao, Y. Qin, Origin of synergistic effects in bicomponent cobalt oxide-platinum catalysts for selective hydrogenation reaction, Nat. Commun. 10 (2019) 1–8, https://doi.org/10.1038/s41467-019-11970-8.

[27] Z. Ferencz, A. Erdőhelyi, K. Baán, A. Oszkó, L. Óvári, Z. Kónya, C. Papp, H.-P. Steinrück, J. Kiss, Effects of support and Rh additive on Co-based catalysts in the ethanol steam reforming reaction, ACS Catal. 4 (2014) 1205–1218, https://doi.org/10.1021/cs500045z.

[28] L. Guczi, D. Bazin, I. Kovács, L. Borkó, Z. Schay, J. Lynch, P. Parent, C. Lafon, G. Stefler, I. Sajó, Structure of Pt-Co/Al_2O_3 and Pt-Co/NaY bimetallic catalysts: characterization by in situ EXAFS, TPR, XPS and by activity in CO (carbon monoxide) hydrogenation, Top. Catal. 20 (2002) 129–139, https://doi.org/10.1023/A:1016363702307.

[29] M.C. Biesinger, B.P. Payne, A.P. Grosvenor, L.W.M. Lau, A.R. Gerson, R.S.C. Smart, Resolving surface chemical states in XPS analysis of first row transition metals, oxides and hydroxides: Cr, Mn, Fe, Co and Ni, Appl. Surf. Sci. 257 (2011) 2717–2730, https://doi.org/10.1016/j.apsusc.2010.10.051.

[30] E. Varga, P. Pusztai, L. Óvári, A. Oszkó, A. Erdőhelyi, C. Papp, H.-P. Steinrück, Z. Kónya, J. Kiss, Probing the interaction of Rh, Co and bimetallic Rh-Co nanoparticles with the CeO_2 support: Catalytic materials for alternative energy generation, Phys. Chem. Chem. Phys. 17 (2015) 27154–27166, https://doi.org/10.1039/C5CP03549J.

[31] J. LUO, M. Meng, X. LI, X. LI, Y. ZHA, T. HU, Y. XIE, J. Zhang, Mesoporous Co_3O_4-CeO_2 and Pd/Co_3O_4-CeO_2 catalysts: Synthesis, characterization and mechanistic study of their catalytic properties for low-temperature CO oxidation, J. Catal. 254 (2008) 310–324, https://doi.org/10.1016/j.jcat.2008.01.007.

[32] A. Ochirkhuyag, A. Sápi, Á. Szamosvölgyi, G. Kozma, Á. Kukovecz, Z. Kónya, One-pot mechanochemical ball milling synthesis of the MnOx: Nanostructures as efficient catalysts for CO_2 hydrogenation reactions, Phys. Chem. Chem. Phys. 22 (2020) 13999–14012, https://doi.org/10.1039/D0CP01855D.

[33] J.C.S. Wu, C.-W. Huang, In situ DRIFTS study of photocatalytic CO_2 reduction under UV irradiation, Front. Chem. Eng. China. 4 (2010) 120–126, https://doi.org/10.1007/s11705-009-0232-3.

[34] J. Baltrusaitis, J. Schuttlefield, E. Zeitler, V.H. Grassian, Carbon dioxide adsorption on oxide nanoparticle surfaces, Chem. Eng. J. 170 (2011) 471–481, https://doi.org/10.1016/j.cej.2010.12.041.

[35] X. Wang, H. Shi, J.H. Kwak, J. Szanyi, Mechanism of CO_2 hydrogenation on Pd/Al_2O_3 catalysts: kinetics and transient DRIFTS-MS studies, ACS Catal. 5 (2015) 6337–6349, https://doi.org/10.1021/acscatal.5b01464.

[36] L. Falbo, C.G. Visconti, L. Lietti, J. Szanyi, The effect of CO on CO_2 methanation over Ru/Al_2O_3 catalysts: a combined steady-state reactivity and transient DRIFT spectroscopy study, Appl. Catal. B Environ. 256 (2019), 117791, https://doi.org/10.1016/j.apcatb.2019.117791.

[37] A. Sápi, G. Halasi, J. Kiss, D.G. Dobó, K.L. Juhász, V.J. Kolcsár, Z. Ferencz, G. Vári, V. Matolin, A. Erdőhelyi, Á. Kukovecz, Z. Kónya, In situ DRIFTS and NAP-XPS exploration of the complexity of CO_2 hydrogenation over size-controlled Pt nanoparticles supported on mesoporous NiO, J. Phys. Chem. C 122 (2018) 5553–5565, https://doi.org/10.1021/acs.jpcc.8b00061.

[38] B. László, K. Baán, A. Oszkó, A. Erdőhelyi, J. Kiss, Z. Kónya, Hydrogen evolution in the photocatalytic reaction between methane and water in the presence of CO_2 on titanate and titania supported Rh and Au catalysts, Top. Catal. 61 (2018) 875–888, https://doi.org/10.1007/s11244-018-0936-z.

[39] B. László, K. Baán, E. Varga, A. Oszkó, A. Erdőhelyi, Z. Kónya, J. Kiss, Photo-induced reactions in the CO_2-methane system on titanate nanotubes modified with Au and Rh nanoparticles, Appl. Catal. B Environ. 199 (2016) 473–484, https://doi.org/10.1016/j.apcatb.2016.06.057.

[40] K. Zhao, L. Wang, E. Moioli, M. Calizzi, A. Züttel, Identifying reaction species by evolutionary fitting and kinetic analysis: an example of CO_2 hydrogenation in DRIFTS, J. Phys. Chem. C 123 (2019) 8785–8792, https://doi.org/10.1021/acs.jpcc.8b11055.

[41] G. Varga, A. Sápi, T. Varga, K. Baán, I. Szenti, G. Halasi, R. Mucsi, L. Óvári, J. Kiss, Z. Fogarassy, B. Pécz, Á. Kukovecz, Z. Kónya, Ambient pressure CO_2 hydrogenation over a cobalt/manganese-oxide nanostructured interface: A combined in situ and ex situ study, J. Catal. 386 (2020) 70–80, https://doi.org/10.1016/j.jcat.2020.03.028.

[42] B. László, K. Baán, Z. Ferencz, G. Galbács, A. Oszkó, Z. Kónya, J. Kiss, A. Erdőohelyi, Gold size effect in the thermal-induced reaction of CO_2 and H_2 on titania- and titanate nanotube-supported gold catalysts, J. Nanosci. Nanotechnol. 19 (2019) 470–477, https://doi.org/10.1166/jnn.2019.15772.

[43] F. Solymosi, J. Kiss, I. Kovács, Adsorption and decomposition of HCOOH on potassium-promoted Rh (111) surfaces, J. Phys. Chem. 92 (1988) 796–803.

[44] T. Kecskés, J. Raskó, J. Kiss, FTIR and mass spectrometric study of HCOOH interaction with TiO_2 supported Rh and Au catalysts, Appl. Catal. A Gen. 268 (2004) 9–16, https://doi.org/10.1016/j.apcata.2004.03.021.

[45] J. Raskó, T. Kecskés, J. Kiss, Formaldehyde formation in the interaction of HCOOH with Pt supported on TiO_2, J. Catal. 224 (2004) 261–268, https://doi.org/10.1016/j.jcat.2004.03.025.

[46] C. Schild, A. Wokaun, A. Baiker, On the mechanism of CO and CO_2 hydrogenation reactions on zirconia-supported catalysts: a diffuse reflectance FTIR study. Part I. Identification of surface species and methanation reactions on palladium/zirconia catalysts, J. Mol. Catal. 63 (1990) 223–242, https://doi.org/10.1016/0304-5102(90)85146-9.

[47] M. Yamamoto, T. Yoshida, N. Yamamoto, T. Nomoto, Y. Yamamoto, S. Yagi, H. Yoshida, Photocatalytic reduction of CO_2 with water promoted by Ag clusters in Ag/Ga_2O_3 photocatalysts, J. Mater. Chem. A. 3 (2015) 16810–16816, https://doi.org/10.1039/C5TA04815J.

[48] L. Lin, S. Yao, Z. Liu, F. Zhang, N.a. Li, D. Vovchok, A. Martínez-Arias, R. Castañeda, J. Lin, S.D. Senanayake, D. Su, D. Ma, J.A. Rodriguez, In situ characterization of Cu/CeO_2 nanocatalysts for CO_2 hydrogenation: Morphological effects of nanostructured ceria on the catalytic activity, J. Phys. Chem. C. 122 (2018) 12934–12943, https://doi.org/10.1021/acs.jpcc.8b03596.

[49] K. Zhao, L. Wang, M. Calizzi, E. Moioli, A. Züttel, In situ control of the adsorption species in CO_2 hydrogenation: Determination of intermediates and byproducts, J. Phys. Chem. C. 122 (2018) 20888–20893, https://doi.org/10.1021/acs.jpcc.8b06508.

[50] W. Chen, B. Zijlstra, I.A.W. Filot, R. Pestman, E.J.M. Hensen, Mechanism of carbon monoxide dissociation on a cobalt Fischer-Tropsch catalyst, Chem. Cat. Chem. 10 (2018) 136–140, https://doi.org/10.1002/cctc.v10.110.1002/cctc.201701203.

[51] Y. Han, C. Liu, Q. Ge, Effect of surface oxygen vacancy on Pt cluster adsorption and growth on the defective anatase TiO_2 (101) surface, J. Phys. Chem. C. 2 (2007) 16397–16404, http://pubs.acs.org/doi/abs/10.1021/jp075602k.

[52] W. Taifan, J.-F. Boily, J. Baltrusaitis, Surface chemistry of carbon dioxide revisited, Surf. Sci. Rep. 71 (2016) 595–671, https://doi.org/10.1016/j.surfrep.2016.09.001.

[53] A. Erdőhelyi, Hydrogenation of carbon dioxide on supported Rh catalysts, Catalysts 10 (2020) 155, https://doi.org/10.3390/catal10020155.

[54] P. Bazin, O. Saur, J.C. Lavalley, M. Daturi, G. Blanchard, FT-IR study of CO adsorption on Pt/CeO_2: characterisation and structural rearrangement of small Pt particles, PCCP. 7 (2005) 187–194.

[55] P. Ferstl, S. Mehl, M.A. Arman, M. Schuler, A. Toghan, B. Laszlo, Y. Lykhach, O. Brummel, E. Lundgren, J. Knudsen, L. Hammer, M.A. Schneider, J. Libuda, Adsorption and activation of CO on Co_3O_4 (111) thin films, J. Phys. Chem. C. 119 (2015) 16688–16699, https://doi.org/10.1021/acs.jpcc.5b04145.

[56] F. Gao, Y. Wang, D.W. Goodman, Reaction kinetics and polarization-modulation infrared reflection absorption spectroscopy (PM-IRAS) investigation of CO oxidation over supported Pd-Au alloy catalysts, J. Phys. Chem. C. 114 (2010) 4036–4043, https://doi.org/10.1021/jp910896k.

[57] J. Kiss, L. Óvári, A. Oszkó, G. Pótári, M. Tóth, K. Baán, A. Erdőhelyi, Structure and reactivity of Au-Rh bimetallic clusters on titanate nanowires, nanotubes and TiO_2 (110), Catal. Today. 181 (2012) 163–170, https://doi.org/10.1016/j.cattod.2011.06.002.

[58] J. Lee, C. Li, S. Kang, J. Park, J.M. Kim, D.H. Kim, Pt nanoparticles encapsulated in CeO_2 over-layers synthesized by controlled reductive treatment to suppress CH_4 formation in high-temperature water-gas shift reaction, J. Catal. 395 (2021) 246–257, https://doi.org/10.1016/j.jcat.2021.01.021.

[59] C. Ahn, H.M. Koo, M. Jin, J.M. Kim, T. Kim, Y.W. Suh, K.J. Yoon, J.W. Bae, Catalyst deactivation by carbon formation during CO hydrogenation to hydrocarbons on mesoporous Co_3O_4, Microporous Mesoporous Mater. 188 (2014) 196–202, https://doi.org/10.1016/j.micromeso.2013.12.035.

[60] C.H. Chen, B.J. Hwang, J.S. Do, J.H. Weng, M. Venkateswarlu, M.Y. Cheng, R. Santhanam, K. Ragavendran, J.F. Lee, J.M. Chen, D.G. Liu, An understanding of anomalous capacity of nano-sized CoO anode materials for advanced Li-ion battery, Electrochem. Commun. 12 (2010) 496–498, https://doi.org/10.1016/j.elecom.2010.01.031.

[61] A.Y. Khodakov, J. Lynch, D. Bazin, B. Rebours, N. Zanier, B. Moisson, P. Chaumette, Reducibility of cobalt species in silica-supported Fischer-Tropsch catalysts, J. Catal. 168 (1997) 16–25, https://doi.org/10.1006/jcat.1997.1573.

[62] S. Schneider, D. Bazin, F. Garin, G. Maire, M. Capelle, G. Meunier, R. Noirot, NO reaction over nanometer scale platinum clusters deposited on γ-alumina: An XAS study, Appl. Catal. A Gen. 189 (1999) 139–145, https://doi.org/10.1016/S0926-860X(99)00263-X.

[63] F. Klasovsky, J. Hohmeyer, A. Brückner, M. Bonifer, J. Arras, M. Steffan, M. Lucas, J. Radnik, C. Roth, P. Claus, Catalytic and mechanistic investigation of polyaniline supported PtO_2 nanoparticles: A combined in situ/operando EPR, DRIFTS, and EXAFS study, J. Phys. Chem. C. 112 (2008) 19555–19559, https://doi.org/10.1021/jp805970e.

[64] X. Wang, N. Li, L.D. Pfefferle, G.L. Haller, Pt-Co bimetallic catalyst supported on single-walled carbon nanotubes: Effect of alloy formation and oxygen containing groups, J. Phys. Chem. C. 114 (2010) 16996–17002, https://doi.org/10.1021/jp102511k.

[65] J. Thiele, R. Belkhou, H. Bulou, O. Heckmann, H. Magnan, P. Le Fèvre, D. Chandesris, C. Guillot, EXAFS study of the crystallographic structure of cobalt thin films on Pt (111), Surf. Sci. 384 (1997) 120–128, https://doi.org/10.1016/S0039-6028(97)00180-5.

[66] X. Wang, N. Li, L.D. Pfefferle, G.L. Haller, Pt-Co bimetallic catalyst supported on single walled carbon nanotube: XAS and aqueous phase reforming activity studies, Catal. Today 146 (2009) 160–165, https://doi.org/10.1016/j.cattod.2009.02.010.

[67] A.A. Tsyganenko, V.N. Filimonov, Infrared spectra of surface hydroxyl groups and crystalline structure of oxides, J. Mol. Struct. 19 (1973) 579–589, https://doi.org/10.1016/0022-2860(73)85136-1.

[68] A. Dannenberg, M.E. Gruner, A. Hucht, P. Entel, Surface energies of stoichiometric FePt and CoPt alloys and their implications for nanoparticle morphologies, Phys. Rev. B - Condens. Matter Mater. Phys. 80 (2009) 1–15, https://doi.org/10.1103/PhysRevB.80.245438.